AIAA Aviation
13-17 June 2016, Washington, D.C.
47th AIAA Plasmadynamics and Lasers Conference

Transient Plasma Impact on Spectra of Flow Disturbances in a Corner Separation Zone at Mach 4.5

Alec W. Houpt[1], Brock E. Hedlund[2], Stanislav V. Gordeyev[3], Thomas J. Juliano[4], and Sergey B. Leonov[5]

Institute for Flow Physics and Control, Department of Aerospace and Mechanical Engineering, University of Notre Dame, Notre Dame, IN, 46556

This work was performed to study the effect on flow disturbances in the corner separation zone of a compression surface with a hypersonic boundary layer caused by a weakly ionized transient plasma generated upstream. Schlieren imaging was used to distinguish the corner separation zone for 15°, 20°, and 25° compression ramps at Mach 4.5 (nozzle exit). A Shack-Hartmann wavefront sensor was used to determine the dominant frequencies of flow oscillations at different locations in the flow field and the resulting effect of repetitively pulsed plasma actuators. A significant rise in amplitudes of high-frequency (>80 kHz) flow perturbations was found when pulsing the plasma at a frequency (100 kHz) higher than the natural dominant frequency of the boundary layer (~65 kHz). The plasma effect was negligible when operated below this frequency (50 kHz). PCB pressure sensors were used to determine the dominant frequencies of pressure oscillations present at the surface on the flat plate and compression ramp inside the separation zone. This technique can potentially be used for active control of the boundary layer condition and supersonic flow structure on the compression surface.

I. Introduction

Scramjet engines provide a reusable and more efficient form of supersonic propulsion as compared to rocket engines. An air-breathing supersonic engine will be used to power high-supsersonic and hypersonic aircraft. These vehicles are expected to operate at high altitudes where the air density is very low in order to ahieve these speeds. This is an advantage for reducing the drag on the vehicle but can cause issues with scramjet operation, one of which is the transition to turbulent flow. Turbulent flow is desired at the inlet of a scramjet so as to reduce flow separation as the flow interacts with the compression surface and helps prevent inlet unstart downstream [1, 2]. The low density associated with high altitudes means that the aircraft will encounter low unit Reynolds number where the transition from a laminar to a turbulent boundary layer does not always occur naturally. Since the incoming flow generally has a low magnitude of freestream disturbances that could promote turbulence the flow needs to be preconditioned by an aerodynamic surface before being ingested. It has been suggested that the most effective mechanism of tripping the flow is the formation of streamwise vorticity within the boundary layer [3, 4, 5, 6].

There are multiple ways that the flow can be tripped to promote the transition to a turbulent boundary layer. The most employed methods include some sort of local barriers, discrete surface roughness, or cross-flow jets. These mechanical methods can augment the mechanisms of instability but have slow response times (orders of magnitude larger than the gas-dynamic time scale) and, in general, are capable of generating a stationary pattern of flow forcing. It can be assumed that unsteady forcing of the boundary layer at the appropriate time scales would be more effective than the steady forcing methods at generating and growing unstable disturbances.

It has been shown that thermal methods, such as plasma, can be used to promote the transition to turbulence [7]. Plasma based flow control uses molecular interactions that transfers energy from an applied electric field to heat and pressure energy via collisional momentum transfer and other molecular process pathways. Plasma actuators

[1] Graduate Student, AIAA Student Member.
[2] Graduate Student, AIAA Student Member.
[3] Research Associate Professor, AIAA Associate Fellow.
[4] Assistant Professor, AIAA Senior Member.
[5] Research Professor, AIAA Associate Fellow.

provide many advantages to the aforementioned methods; faster response time, no moving parts, a robust installation flush with the surface, adjustable frequency to match flow characteristics, and the ability to generate unstable disturbances. Plasma flow control has been studied extensively with most studies focusing on AC or pulse driven Surface Dielectric Barrier Discharge (SDBD) plasmas [8, 9, 10, 11, 12, 13]. These types of discharges are limited by the repetition frequency and power deposition rate. The power deposition and power density are typically too low for SDBD to have much of an effect on high-speed flows.

There have also been studies done with plasma flow control in high-speed applications [11, 14, 15, 16, 17, 18, 19, 20, 21]. Plasma was generated in numerous ways including DC, AC, RF, microwave, arc, corona, and spark electric discharges, as well as laser induced breakdown, and applied to subsonic and supersonic flow regimes. The main focus of most applications of plasma actuators is in viscous drag reduction and boundary layer separation control in low-speed flows while supersonic and hypersonic applications focus on dynamic stall control, boundary layer transition, shock wave modification, and reduction of wave drag. Purely thermal methods of flow control rely on energy addition from bulk heating of the flow which would require a high plasma power budget for high-speed flows; comparable to the flow enthalpy.

Many studies have been done on the importance of the non-uniform nature and transient behavior of plasmas and how they can be utilized in controlling the boundary layer [14, 22, 23, 24, 25, 26, 27, 28]. One of the most important characteristics of the plasma is its non-uniformity or the ability to generate hot spots due to localized heating. This interacts with the flow in a similar manner to physical obstacles by forcing the flow which generates vortices and wavelets that convect along with the flow. Rapidly modulating the discharge energy may promote the transition to turbulence. A computational study was done on the effect of thermal perturbations, which can be generated by plasma, on a flat plate boundary layer in Mach 1.5 flow [7]. Steady and pulsed surface temperature perturbations were modeled. The steady localized wall heating generates a flow perturbation that slowly decays as it travels. The repetitive pulsing of wall heating at $100\ kHz$ showed that nonlinear vortex interactions cause perturbations to significantly grow as they travel downstream, with fluctuation levels reaching as high as 20% of the free stream velocity. This type of flow is highly susceptible to secondary instabilities thus showing for the first time that thermal perturbations, such as those created by electrical discharges, can be used to control the transition to turbulence in high-speed flows.

The generation of a near-surface weakly ionized plasma by high-current short-pulse discharge is considered for use in promoting turbulence upstream of the separation bubble in a corner of a compression surface in supersonic/hypersonic flow. The multitude of advantages provided by plasma actuators compared to mechanical methods makes them a prime candidate for study and implementation into future air-breathing supersonic combustion engines. The boundary layer receptivity and resulting effect that plasma actuators have on the corner separation bubble is the main focus of this study. A plasma generator that can feasibly produce a pointwise, near-surface discharge at frequencies as high as $> 50\ kHz$ in low pressure, high-speed flow is studied experimentally. The structure and dynamics of gas pressure and density perturbations generated as well as the boundary layer receptivity to the plasma-based perturbations are studied using optical techniques and pressure sensors.

Despite a large interest in this scientific field the feasibility and the efficiency of practical implementation of plasmas for a high-speed flow control remains unclear. One of the important goals of this work is to determine the benefits and drawbacks of the plasma-based approach for control of boundary layer state and separation processes in supersonic and hypersonic flows.

II. Test Approach

A. Experimental Facility Description

Testing took place at the University of Notre Dame in the high enthalpy arc tunnel, ACT-1, in Mach 4.5 flow. Figs. 1 and 2 below illustrate the test section arrangement and pictures of the model within the test facility respectively. The test conditions consisted of: Reynolds Number $Re_L \approx 4 \cdot 10^6\ m^{-1}$; stagnation temperature $T_0 = 300\ K$ (cold flow) and $1800\ K$ (hot flow); stagnation pressure $P_0 \approx 0.8\ bar$; flow enthalpy $h \cdot \dot{m} \approx 10\ kW$ (cold flow) and $50\ kW$ (hot flow). "Cold flow" and "hot flow" will be used to distinguish between low-enthalpy and high-enthalpy tests respectively. The experimental model consisted of a flat plate with a sharp leading edge at an angle $\alpha = 15°$. The second wedge was mounted on top of the flat plate to form the compression ramp at a variable angle β. In total, the model measured: length $L = 229\ mm$, width $W = 102\ mm$, and height $H = 19\ mm$. $62\ mm$ upstream of the ramp, a row of electrodes was mounted spanwise through the model. Insulated by a ceramic insert, the electrodes were used to generate a plasma discharge on the top surface of the model. This placement is pointed out in Figs. 1 and 2.

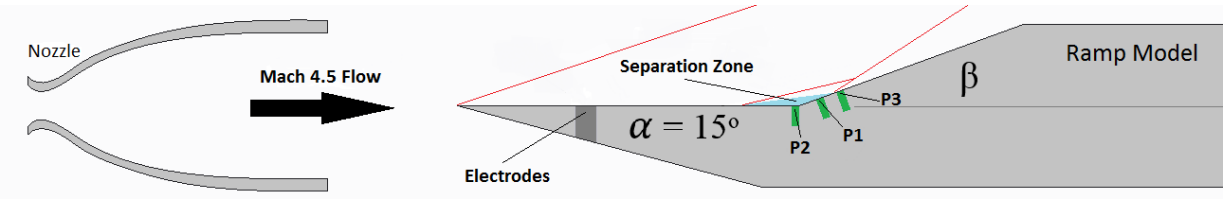

Fig. 1. Side view of experimental arrangement.

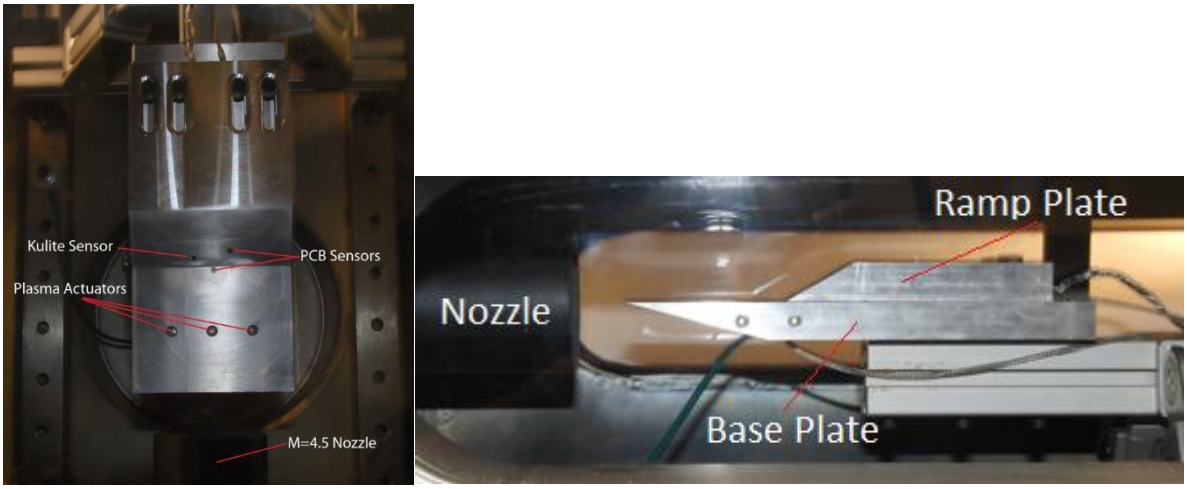

Fig. 2. Model in the test section of ACT-1 at the University of Notre Dame.

Tests lasted up to 1 second, during which the arc heater operated for $0.3\ s$ (for hot flow) and plasma generation lasted $0.1\ s$. The model allows for variations in ramp angles $\beta = 15° - 25°$ to initiate flows with or without the corner separation zone. To establish a baseline and consistency in flow characteristics from one test to the next, data was collected before, during, and after plasma actuation. Instrumentation in the sequence of data collection included a schlieren imaging system, high-speed wave front sensor, high speed camera, high sensitivity pressure transducers, and probes to measure current and voltage of the electrical discharge. The tests performed were:

- test 1: no plasma operation for baseline characteristics;
- test 2: pulse-periodic operation of plasma in the flow.

Both Kulite and PCB pressure sensors were selected to provide physical measurements of the pressure and perturbation frequencies within the corner separation zone. A Kulite XCQ-080 miniature pressure transducer provided an absolute pressure measurement within the separation zone at location P1 in Fig. 1. This sensor however, has a limited range of frequency capabilities and measurements are limited to 15 kHz and below, allowing the measuring the average surface pressure dynamics during the test. A sample of the Kulite sensor measurements is shown in Fig. 3. Pressure amplitude, measured on the ramp at P1 by a Kulite sensor provides pressure profiles for both cold and hot flow tests below.

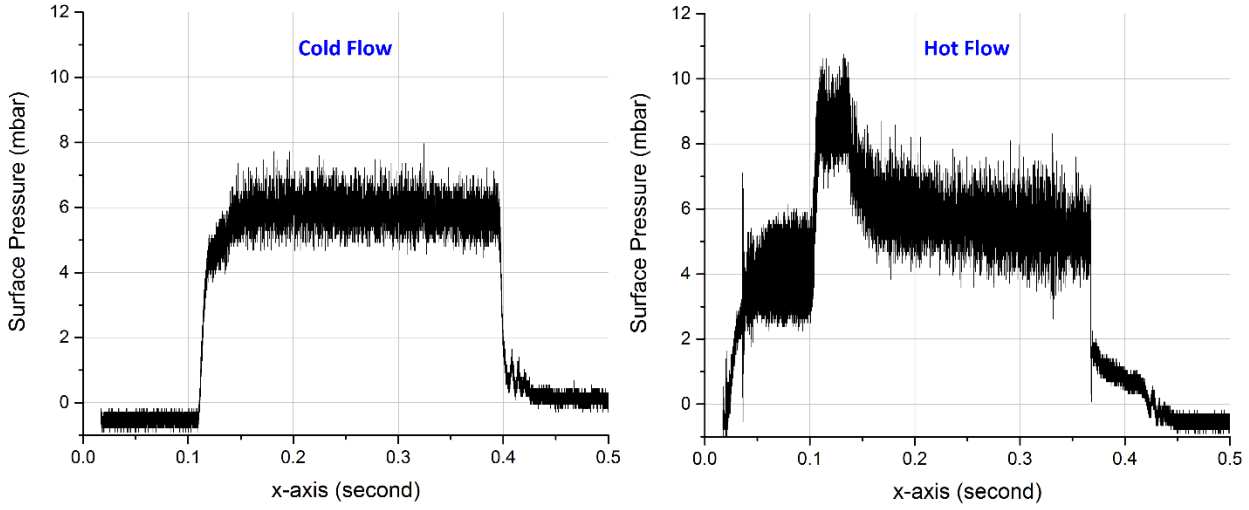

a. b.

Fig. 3. Pressure data on ramp surface for (a) cold and (b) hot flow tests.

In Fig. 3a, the cold flow profile reflects the steady flow of nitrogen gas activated for 0.3 seconds. Fig. 3b shows the time sequence, beginning with an initial flow of argon gas for approximately 80 ms in order to initiate the arc. The flow of argon cuts out around 0.125 s and transitions the arc operation to nitrogen only, thus reducing the surface pressure for the remaining 250 ms of nitrogen flow. This data shows the extreme case for the highest pressure to expect in the separation bubble and act as a guide for the other test conditions.

Two PCB (132 series) microsensors located at P2 and P3 in Figs. 1 and 2 (only for the $\beta = 25°$ case) provided high frequency pressure measurements in the corner separation zone. The location of these sensors (on the flat plate and ramp respectively) was chosen to provide samples of perturbations on both surfaces.

B. Estimation of Natural Instability Frequency

The most-amplified naturally occurring disturbances in the test article's boundary layer were estimated from Linear Stability Theory results for a flat plate as follows. Fig. 3h in [29] presents the non-dimensionalized frequency F as a function of $(Re_{x,e})^{1/2}$ for an adiabatic flat plate at Mach 4.5. The non-dimensional frequency F is defined as:

$$F \equiv \frac{2\pi f}{U_e Re_e}$$

where f is the disturbance frequency, U_e is the boundary-layer edge velocity, and Re_e is the unit Reynolds number at the boundary-layer edge.

For a flat plate at zero angle of attack, the unit Reynolds number at the boundary-layer edge equals the freestream unit Re; for these test conditions, $Re_e = 4.0 * 10^6 /m$. The Reynolds number based on the distance from the leading edge to the actuators ($x = 0.10\ m$) and boundary-layer edge conditions, $Re_{x,e}$, for this test condition is thus $4.0 * 10^5$. According to Fig. 3h in [29], for $(Re_{x,e})^{1/2} = 630$, $F \approx 7.1 * 10^{-5}$ then the dominant frequency is $f \approx 77\ kHz$. The low-enthalpy case has an approximately adiabatic wall. In the high-enthalpy case, the wind tunnel run time was too short to reach an adiabatic wall, so the relatively cold wall would result in a thinner boundary layer and somewhat higher disturbance frequency [30].

Neutral stability curves for this case are presented in Fig. 10.5 of [30]. The point corresponding to $(Re_{x,e})^{1/2} = 630$ and $F \approx 7.1 * 10^{-5}$ is well within the unstable region for first-mode (Tollmien-Schlichting) waves. Therefore, first-mode waves with frequencies on the order of $70 - 80\ kHz$ were anticipated for the flat-plate boundary layer in the absence of plama actuation.

C. Approach to the Plasma Actuator Design

The fast development of a gas dynamic instability can be promoted by the introduction to the system of an oscillation of pressure or gas density, with a proper frequency, to the boundary layer. The main method for doing so

is a modulation of the electrical power deposited to the plasma. This method might not be fast enough because the response time is limited by the gas dynamic time scale, related to a characteristic length of a few centimeters. At the same time, a modulation of electrical parameters of the plasma might initiate much faster kinetic processes in the gas flow.

Over the last few years, kinetic mechanisms of "rapid heating" resulting from energy transfer from internal molecular energy to translational/rotational temperature, on a sub-microsecond time scale, have been analyzed in great detail [31, 32, 33]. This suggests that rapid heating, caused primarily by the quenching of N_2 excited electronic states by oxygen, $N_2^* + O_2 \rightarrow N_2 + O_2$, would result in significant pressure overshoot in the plasma zone [34]. The process of gas dissociation may deliver even faster pressure elevation, although with a lower overall efficiency. In a multicomponent gas (air), the gas pressure can be represented by the sum of partial pressures of each component. The equation takes into account the ionization with degree α and the dissociation of a molecular gas with degrees δ_k for the k-component (N2, O2, at least). For the dissociation of multiatomic molecular gases the dissociation degree is defined as $\delta_k = \frac{\sum_i N_{ki} - N_k}{N_k}$, where i-species are originated due to k-species dissociation. Thus the gas pressure is

$$P = k_B \cdot \sum_{k=1}^{m} N_k \cdot T_k \approx\approx k_B \cdot (N_{N2} + N_{O2}) \cdot \left((1 + (1-\chi)\cdot\delta_{N2} + \chi\cdot\delta_{O2})\cdot T_g + \alpha\cdot T_e\right)$$

Here k_B is the Boltzmann constant and χ the molar fraction of molecular oxygen in the gas. Nitrogen dissociation is negligibly small at these conditions. If only fast processes are considered (frequency $f \geq 10^5\ Hz$), for the rough estimation the gas density can be posed as a lesser variable than the gas temperature and pressure. After simplification the pressure dynamics can be expressed by the following formula:

$$\frac{dP}{dt} \approx k_B \cdot (N_{N2} + N_{O2}) \cdot \left((1 + \chi\cdot\delta_{O2})\cdot\frac{\partial T_g}{\partial t} + \chi\cdot\frac{\partial\delta_{O2}}{\partial t}\cdot T_g\right)$$

Note, that the derivative of the dissociation degree can be calculated through a dissociation reaction rate coefficient k^d_{ki} (2^{nd} order). :

$$\frac{\partial\delta_k}{\partial t} = \frac{1}{N_k}\cdot\sum_i\frac{\partial N_{ki}}{\partial t} = \sum_i (k^d_{ki}\cdot N_k - k^r_{ij}\cdot\frac{N_{ki}\cdot N_{kj}}{N_k})$$

where the recombination processes with rate coefficients k^r_{ij} could be neglected with fast temperature elevation.

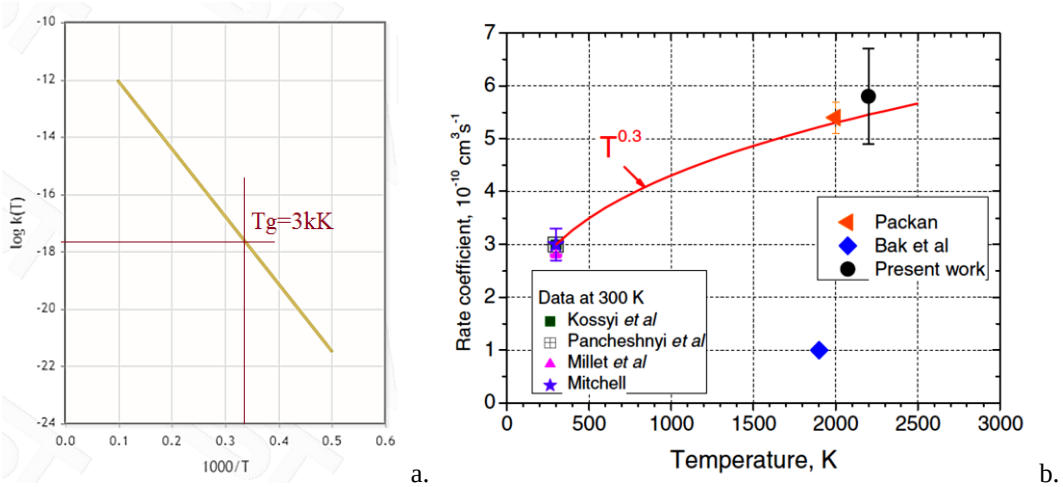

a. b.

Fig. 4. Thermal dissociation rate constant. a – reaction O2 (thermal) = O + O [k]=m^3/s [35]; b – reaction N2*+O2=N2+O+O - quenching rates of N2(C) by O2 [36].

The measurements performed in a nanosecond duration discharge [36] confirm that the ultrafast dissociation of molecular oxygen is mainly due to the quenching reaction of N2(B) and of N2(C) by oxygen. The fraction of dissociated oxygen reaches about 50% after 20 ns. Both the gas temperature evolution and oxygen density are in good

agreement with the ultrafast mechanism simulations of Popov [32, 37, 38]. The fraction of energy spent on dissociation of oxygen is about 35%, and the fraction of energy spent on gas heating is about 21%. Figure 4 presents data on reaction rate constants for thermal dissociation of oxygen and oxygen dissociation in low-temperature pulsed plasma. It is well seen that a thermal dissociation of oxygen does not play a significant role in pressure elevation even at gas temperature $T_g \approx 3kK$, compared to the non-equilibrium dissociation in plasma. The effect of the plasma-based dissociation might be >10^3 times higher than one due to the thermal mechanism. To realize such a mechanism, the plasma should be organized in a proper way. It is also important that in the case of a plasma kinetic mechanism the upper boundary of the frequency of pressure oscillations is not limited by a slow, purely thermal, process.

Existing data [39, 40] allows suggestion that the most effective frequency of artificial disturbances for tripping the boundary layer for excitation of the first mode of BL disturbances at $M = 5$ is $f = 100 - 200\ kHz$. For a proper optimization of the system, the frequency of plasma operation has to be adjustable over a wide range. Previously, data was collected with isolated roughness elements installed in one line in the spanwise direction with 5 to 25 mm spacing [4]. Based on suggestion to produce the local instant gas temperature increase $\Delta T \approx 10^2 - 10^3\ K$ the average electrical power of each actuator should be in the range of $P = 100 - 500\ W$. The duration of each plasma pulse should be of microsecond or submicrosecond scale to produce pointwise disturbances. A low level of gas density in a hypersonic boundary layer flow may cause an issue because in a low gas density environment the discharge strives to transit to a glow type discharge where the power density becomes too low for any observable effect. Preliminary tests [41] indicate that it is possible to generate filamentary plasma at the molecular concentration of $n > 2 \times 10^{17}\ cm^3$ using a simple two-electrode scheme.

The Shallow Cavity Discharge actuator [41] has been used in these tests. It is flush mounted, with a size of a few millimeters, and can be installed on the metallic surface of the model. It has the proper discharge geometry, reasonably low applied voltage, and a sufficient level of the disturbances excited. Time resolved image of the SCD discharge in $M = 4.5$ flow taken by the Andor iStar ISSD camera is shown in Fig. 4. At $f = 50 - 100\ kHz$, the discharge works as a push-pull plasma mini-jet. At lower frequencies of repetition the second operation mode was observed, currently considered as a cathode sheath pattern, where a rather thin layer of plasma covers most of the model surface. The cathode sheath is where a major part of the electric power is released [42] that is potentially beneficial for the BL control.

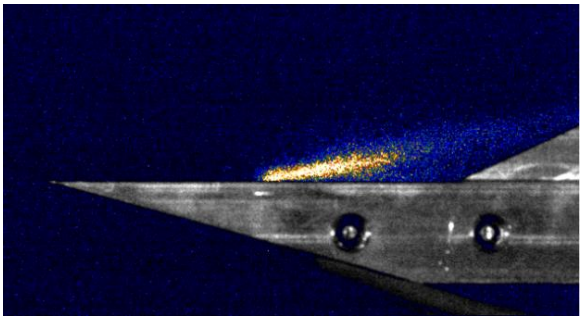

Fig. 5. SCD in $M = 4.5$, $P = 4\ mBar$ flow in plasma mini-jet operation mode. Exposure 1μs, delay time 3 μs (within the electric pulse).

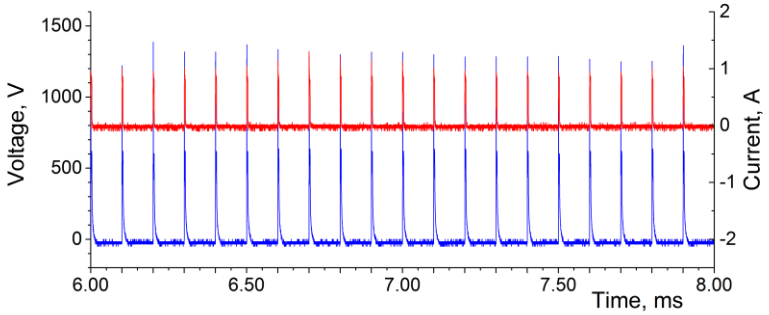

a.

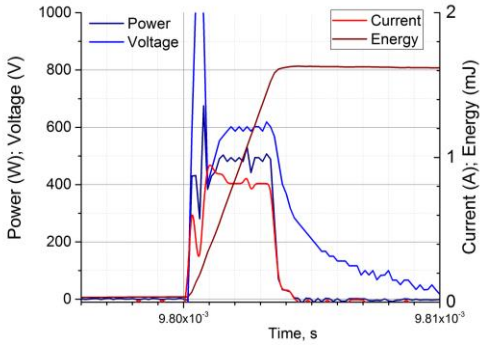

b.

Fig. 6. Voltage –current time series of the SCD operation at $f = 100\ kHz$ (a); calculation of the discharge pulse power and energy (b).

Typical records of the electric parameters in M=4.5 flow are shown in Fig. 6a for a frequency of repetition $f = 100\ kHz$. The pulse energy and average power were calculated based on these data, as it is shown in Fig. 6b. The discharge parameters were as follows: frequency of repetitions $f = 10 - 100\ kHz$; pulse duration $t < 3\ \mu s$; voltage $U < 2\ kV$; pulse energy $E = 1.2 - 2\ mJ\ /unit$; average power $W_{av} < 500\ W$. Three units of SCD have been arranged in the model.

D. Aero-Optical Measurements

Aero-optical diagnostic measurements were performed using a high-speed Shack-Hartmann wavefront sensor [43]; a schematic of the experimental setup is shown in Fig. 7. The laser beam was expanded to a 50-mm-diameter collimated beam and passed along the spanwise direction over the corner region of the model mounted in the test section. The spanwise beam propagation was chosen for two reasons. First, the flow is expected to be primarily spanwise-uniform. Second, as the beam traverses the 4-inch-long region of the flow, aero-optical distortions become stronger thus improving the signal-to-noise ratio [44]. After exiting the test section, the beam is reflected off the return mirror, which sends the beam back along the same path. This so-called double-path setup further amplifies the aero-optical signal by a factor of two, as the beam traverses through the flow of interest twice, and also simplifies the optical setup. The returning beam is split off using a cube beam splitter, sent though a contracting telescope, which reduces the beam size to 12.5 mm in diameter, and recorded by a Phantom v1611 high-speed digital camera. The camera had a 38 mm focal length, 70x60 lenslet array with 0.3-mm-pitch with 100% fill ratio, attached to it. After passing through the lenslet array, the beam was split into subaperture beams and focused on the camera sensor, creating a series of dots. To achieve the high, 531 kHz, sampling rate, only a small portion of the image (128×64-pixel) was acquired (Fig. 8) for the full duration of the tunnel run. This image size corresponds to a 15×7 mm measurement region over the model, with 1.2 mm spacing between the dots.

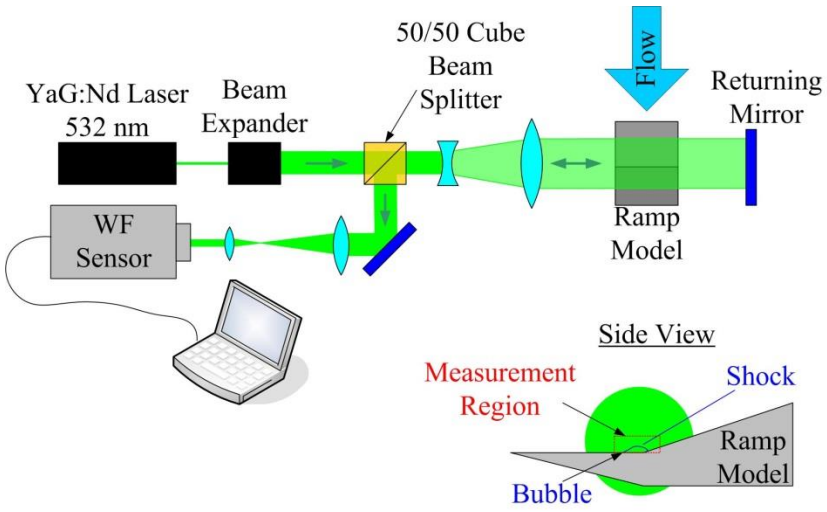

Fig. 7. Schematic of optical set-up.

It is important to note that all aero-optical measurements are non-intrusive by nature, sensitive to the density field only, provide good spatial resolution and limited in temporal resolution only by the digital camera technology. Comparing to other optical diagnostics, like schlieren or shadowgraph techniques, wavefront measurements provide additional advantages. The light from each lenslet is focused on a digital sensor, increasing the dot intensity, so wavefront measurements can be done with less-powerful lasers. A location of the dot is typically extracted with better than 0.1 pixel resolution using centroiding algorithms [45], providing accurate measurements of the deflection angle over the subaperture, since the displacement of each dot is proportional to the subaperture-averaged deflection angle. The time series of the deflection angles carry information about the temporal characteristics of the density field over different spatial locations across the laser beam. The wavefront sensor simultaneously measures both streamwise (X-) and wall-normal (Y-) components of the deflection angle; this is in contrast to Schlieren, where wavefront changes are measured along only one fixed direction. The 2-component deflection angle is a local gradient of the wavefront, so knowing both components of the deflection angle the wavefront (or equivalently, Optical Path Difference or OPD) can be computed. OPD is proportional to the spanwise-integrated density field, $OPD(x,y,t) = K_{GD}\int \rho'(x,y,z,t)dz$ [46], where K_{GD} is the Gladstone-Dale constant, and knowing OPD, the amplitude of the density fluctuation over a subaperture can be estimated [44]. In contrast, time-resolved Schlieren images provide good spatial and temporal information, but density information is not easily extracted from them. Finally, the wavefront measurements using the Shack-Hartmann sensor are fairly insensitive to mechanical vibrations, imposed on the test section, the model and different components of the set-up [46].

To better visualize the relation between the spatial distribution of the deflection angles, measured by the wavefront sensor, and the flow features, the same optical setup was also used to collect high-speed shadowgraph movies. To do this, the lenslet array was removed and distorted intensity patterns were recorded at the same sampling speed of 531 kHz over the same 64x128 area. The representative shadowgraph image with an overlaid dot pattern from a time-averaged Shack-Hartmann wavefront sensor images is shown in Fig. 8. Several flow regions, indicated by yellow circles in Fig. 8, were selected to investigate the temporal dynamics and the sensitivity to the plasma generators: point BL2 is inside the separated bubble, A2 and A3 correspond to the unsteady shock over the separation bubble, and A4 is in the outside portion of the flow downstream of the plasma generators. In-house software was used to extract the temporal motion of the dots and to convert this into a time series of the deflection angles.

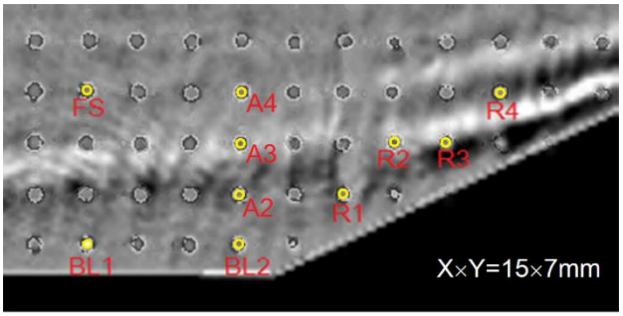

Fig. 8. Shadowgraph image with an overlaid dot pattern to identify different flow regions near the model corner.

III. Test Results

For all of the tests it was important to distinguish the formation, size, and stability of the corner separation zone. High-speed schlieren frame sequence and high-definition schlieren images in $M = 4.5$ flow were taken for this purpose and can be seen in Figs. 9 and 10 respectively. It was observed that the corner separation bubble forms within $15\ ms$ of the flow starting and holds its position stable, with expected oscillations due to boundary layer fluctuations observed. It can be seen in Fig. 9 that for the $15°$ ramp a small corner separation is produced most likely due to a small negative angle of attack. Corner separation begins to become visible at $\beta = 20°$ and is more prominent at $\beta = 25°$. The high-definition schlieren image in Fig. 10 was taken for the $20°$ ramp angle to better distinguish the corner separation zone for this case since it is an intermediate case.

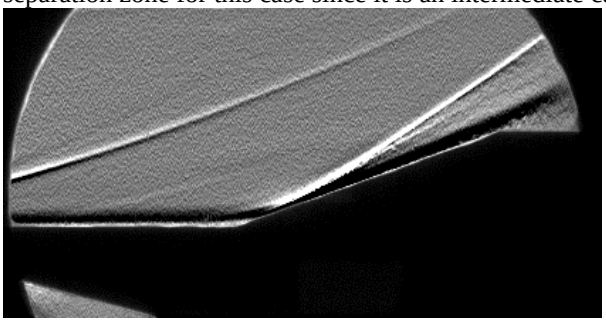
a.
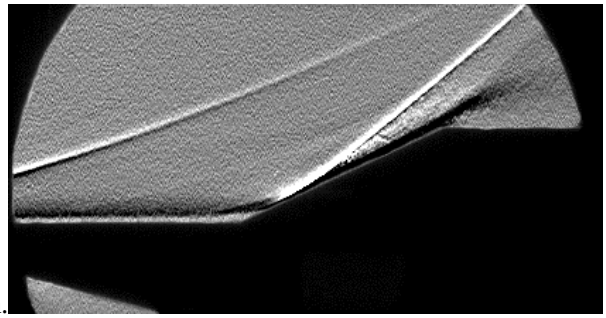
b.
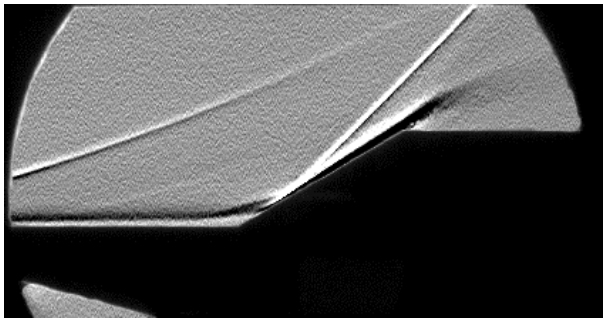
c.

Fig. 9. Schlieren image from high-speed video (10,000 fps) without plasma and ramp angle $\beta = 15, 20,$ and $25°$ (a, b, and c respectively).

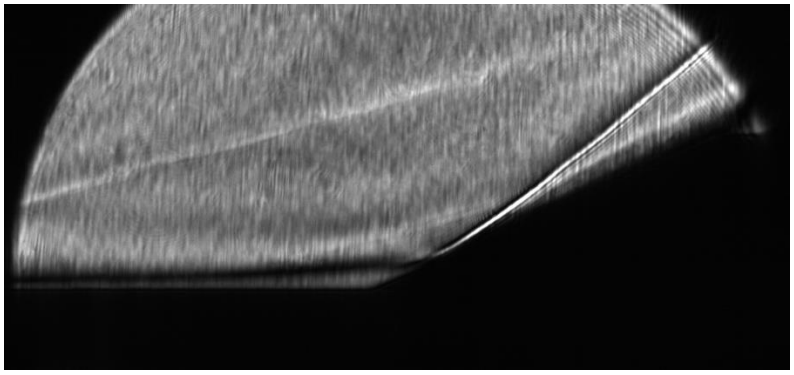

Fig. 10. High-definition schlieren image without plasma operation and ramp angle $\beta = 20°$

Test 1 included substantiating the aero-optical measurements with pressure sensors since the optical methods cannot measure what is happening at the surface. The ramp angle was also varied to determine the effect β and the presence of corner separation had on the flow disturbances. At the surface, pressure data was collected at three locations for $\beta = 25°$ in order to gather pressure amplitude (shown in Fig. 3) and flow perturbations using AC coupled PCB sensors.

Using the PCB sensors it is possible to gather perturbation frequency measurements far beyond 100 kHz. The two PCB sensors, mounted at P2 and P3 (see Fig. 1) detected flow perturbations on both the flat plate and ramp surfaces. Mounting these sensors proved difficult due to the thin geometry of the ramp at the leading edge of the wedge. This limited the use of the two ramp mounted sensors to the 25° configuration. The spectra of flow perturbations for both locations are shown in Fig. 11.

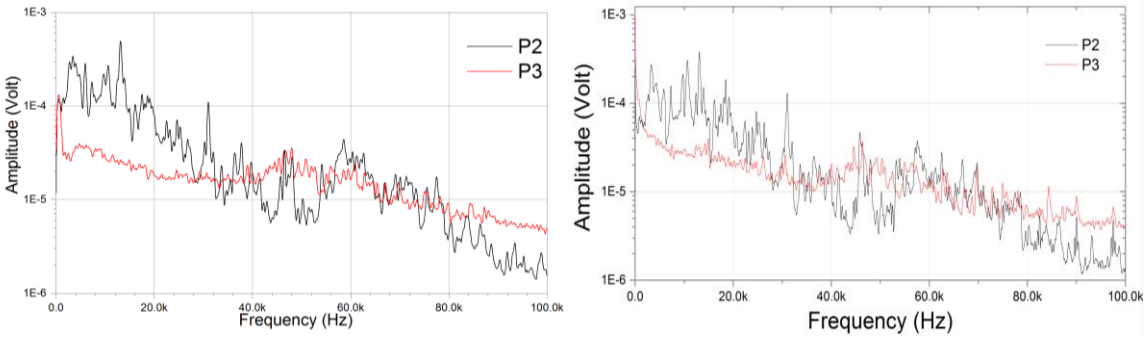

Fig. 11. Spectra of flow disturbances measured by pressure sensors in (a) cold flow and (b) hot flow.

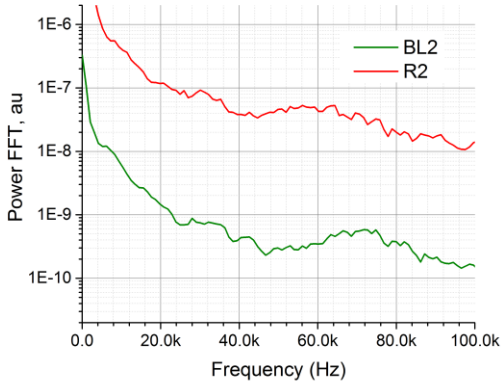

Fig.12. FFT spectra of optical density perturbations taken close to the pressure sensors location, points BL2 and R2.

The two sensor locations provide different spectra. This may be due to different interactions occurring at each surface location and sensor. P3 is located slightly behind the shock generated by the ramp, which may explain different perturbation frequencies. It is evident in Fig. 11 that a dominating frequency of $\sim 60\ kHz$ is detected by P2 in both low and high enthalpy tests. Recurring spikes at approximately $15,\ 30$, and $45\ kHz$ as detected by the sensor at P2 in Fig 11 can be considered as instrumentation effects and the resulting harmonics.

Figure 12 demonstrates the optical density fluctuations spectra taken by the aero-optical technique to be compared to the pressure sensor dataset. Two lines of observation have been chosen to be close to the locations of the pressure sensors. The major frequency of disturbances, measured by two techniques is similar including some shift of the frequency "bump" to lower values on the ramp compared to the boundary layer.

Test 2 studied the effect of pulse-repetitive SCD operation on the spectrum of flow perturbations in and near the corner separation zone. Deflection-angle spectra obtained using the high-speed Shack-Hartmann wavefront sensor were analyzed at the locations indicated in Fig. 8. Early results showed [47] that SCD operation affects the spectra only slightly if the repetition frequency is less than the dominant frequency of the first-mode instability, $F_1 = 60 - 80\ kHz$. Operating at a frequency greater than F_1 produces significant changes in the spectra of disturbances.

As mentioned above, the wavefront sensor measures horizontal (X) and vertical (Y) components of the wavefront gradient. Isotropic flows generally display close to equal magnitudes of the wavefront gradient in the horizontal and vertical directions. The flow considered in this study is expected to have larger magnitudes of deflection angles in the wall-normal (Y) direction compared to the streamwise (X) direction as a result of the larger density gradients in the wall-normal direction. This in turn amplifies the effect that the plasma has on exciting the higher frequency disturbances and results in larger magnitudes of deflection angles which can again be seen by comparing the two figures.

Figures 13a-d show data for plasma actuation at frequency $100\ kHz$ for two points in incoming boundary layer and two points near the compression ramp. Each test included measurements of $0.1\ s$ prior to plasma actuation, and $0.1\ s$ during plasma operation. There appears to be a small effect of the plasma in the boundary layer at point BL1 (see Fig. 8). In the point BL2, Fig.13b, where the amplitude of perturbations is higher, the amplitude of high-frequency disturbances, larger than $80\ kHz$, increases. However, looking at Figs. 13c and 13d gathered for the ramp locations, it can be seen that these high-frequency disturbances were excited causing a significant reduction of the major frequency oscillations.

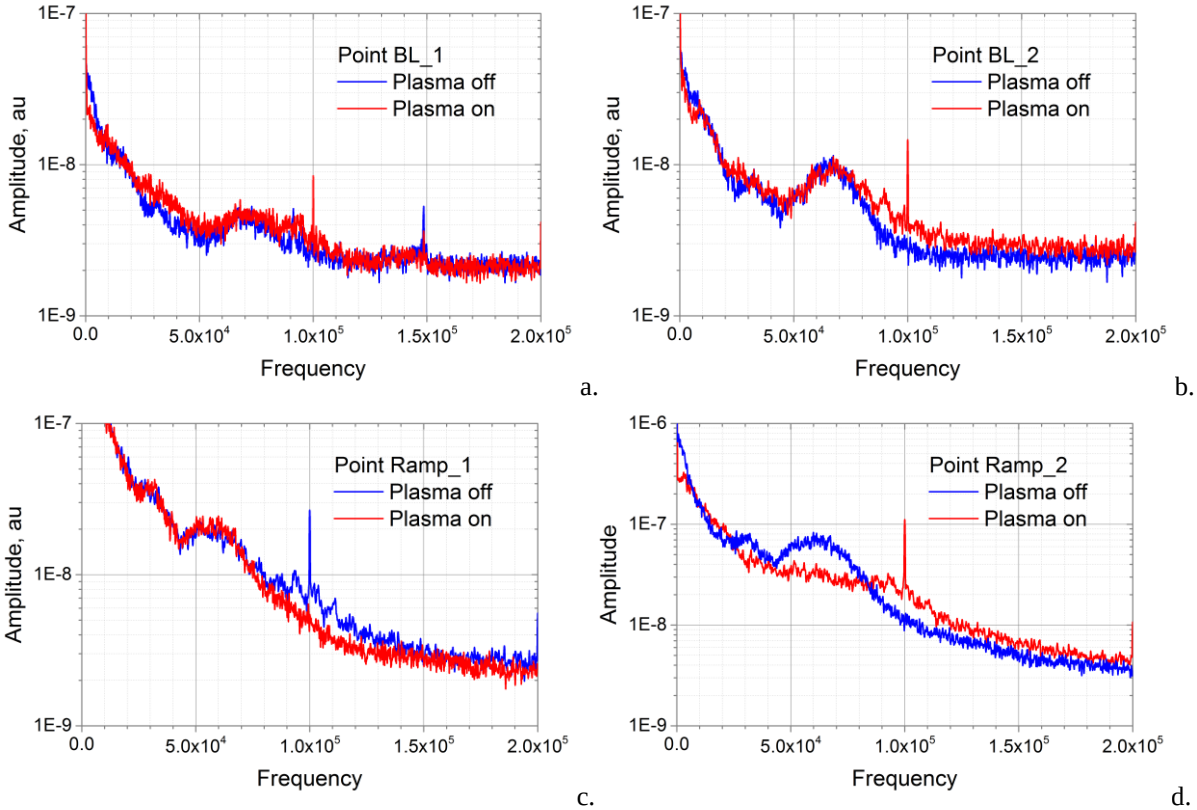

Fig. 13. Spectra of flow disturbances. Y-component of the deflection-angle spectra, plasma excitation $f = 100\ kHz$. (Fig. 8 for reference)

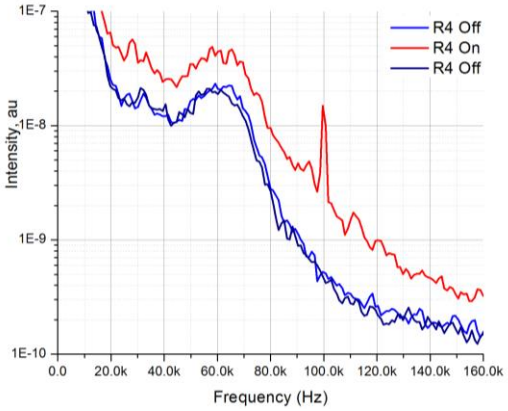

Fig. 14. Spectra of flow disturbances on the ramp, point R4 (Fig. 8 for reference).

Fig. 14 displays the spectra of flow perturbations in the point Ramp_4 with the largest observed plasma effect. Here the data are presented for three time periods: befor the plasma actuation, at plasma on and after it turned off. This was done to ensure that flow parameters did not change during operation. Point R4 lies on the compression ramp and is very near the root part of the shock generated by the ramp. The magnitude of the flow disturbances were increased for all observed frequencies and even extends beyond $100\ kHz$. The resulting amplification of flow perturbations at R4 due to the operation of the SCD actuators is $A/A_0 = 2 - 8$.

IV. Conclusion

There is a range of parameters that can be utilized for plasma-based boundary layer transition control in high-speed flows. It seems that with a satisfactory geometric/periodic arrangement of the plasma actuators, the optimum forcing frequency is dependent on the dominant frequency of disturbances present in the flat plate boundary layer. The freestream noise and freestream Reynolds number determine the dominant frequencies in the boundary layer.

The generation of a constricted plasma in a low-density gas, characteristic of high-speed boundary layers, is of utmost importance in actually being able to affect the flow structures. The shallow cavity discharge has been shown to fit this need and is still being studied to define the limits of its operation. The hope is to be able to push its operating frequency to $200\ kHz$ while maintaining its power density such that it can be utilized in a wide range of high-speed flows into the hypersonic range. The specific geometry of the SCDs used, a one-dimensional array of plasma elements in the spanwise direction with individual control of each element, has demonstrated its effectiveness in exciting high-frequency disturbances within the boundary layer. These tests have also demonstrated the feasibility of high repetition rate plasma operation in low-density, high-speed flow.

Employing pressure sensors with high-frequency capabilities allowed for the verification of the results obtained from the aero-optical techniques. The Shack-Hartmann sensor collected data about the flow filed, while the pressure sensors can only collect data at the surface. It is important to gather both in order to have a better understanding and verification of the results. Looking at all of the data collected it is reasonable to conclude that hypersonic boundary layers are sensitive to highly transient plasmas. Active tripping of the boundary layer by electrical discharges can be done for a wide range of flow conditions so long as the forcing frequency is higher than the dominant frequency of perturbations present in the boundary layer; $f > F_1$. The aero-optical techniques employed have high potential for use in high-speed flows due to the ability to gather data in a non-intrusive way at high-frequencies (as high as $1\ MHz$), with high spatial resolution. Utilizing optical methods and surface mounted pressure sensors it is possible to determine the flow perturbations in the flow field as well as on the surface.

The spectra of pressure oscillations were gathered from surface mounted pressure sensors. The frequencies observed for cold and hot flows were very similar, but of different magnitudes. It was expected to see higher frequencies in the heated runs due to the higher velocity, but it is not readily apparent how the dominant frequency is affected since it is a function of the Reynolds number and therefore depends on more flow properties than the velocity. It was also observed that the spectra varied depending on the location of the sensor. This reasoning is unclear at the moment as it is possible that shock wave boundary layer interactions or shock-wall interactions could have an effect

on the flow structure. Varying the ramp angle had little effect on the dominant frequencies present on the flat plate in the separation bubble, or boundary layer in the $\beta = 15°$ case.

Going forward it is proposed to gather more data for varying flow conditions, Mach 6 and 9 in the ACT-1 high-enthalpy facility with potential to apply the same concepts in the SBR-50 supersonic tunnel also at the University of Notre Dame, with more diagnostic techniques to be utilized. In the near future laser differential interferometry will be used to gather more non-intrusive measurements with high temporal and spatial resolution to continue to determine the full view of the flow structure and dynamics.

Acknowledgment

The current work is supported by the FlowPAC Institute at the University of Notre Dame. A portion of this work (design of the SCD plasma actuator [41]) was previously supported by MBDA-France (Mr. Francois Falempin supervision).

References

[1] A. Valdivia, K. B. Yuceil, J. L. Wagner, N. T. Clemens and D. S. Dolling, "Control of Supersonic Inlet-Isolator Unstart Using Active and Passive Vortex Generators," *AIAA Journal*, vol. 52, no. 6, pp. 1207-1218.

[2] Y. Wu, S. Yi, L. He, Z. Chen and Y. Zhu, "Flow Visualization of Mach 3 Compression Ramp with Different Upstream Boundary Layers," *Journal of Visualization*, vol. 18, pp. 631-644, 2015.

[3] S. A. Berry, R. J. Nowak and T. J. Horvath, "Boundary Layer Control for Hypersonic Airbreathing Vehicles," in *34th AIAA Fluid Dynamics Conference, AIAA-2004-2246*, Portland, Oregon, 28 June-1 July, 2004.

[4] S. Schneider, "Effects of Roughness on Hypersonic Boundary-Layer Transition," *Journal of Spacecraft and Rockets*, vol. 45, no. 2, pp. 193-209, 2008.

[5] E. Reshotko and A. Tumin, "Role of Transient Growth in Roughness-Induced Transition," *AIAA Journal*, vol. 42, no. 4, pp. 766-770, April 2004.

[6] M. Choudhari, F. Li and J. Edwards, "Stability Analysis of Roughness Array Wake in a High-Speed Boundary Layer," in *47th AIAA Aerospace Sciences Meeting, AIAA-2009-170*, Orlando, Florida, 5-8 January, 2009.

[7] H. Yan and D. Gaitonde, "Effect of Thermally Induced Perturbation in Supersonic Boundary Layers," *Physics of Fluids*, vol. 22, no. 064101, pp. 1-17, 2010.

[8] I. V. Adamovich, J. Little, M. Nishihara, K. Takashima and M. Samimy, "Nanosecond Pulse Surface Discharges for High-Speed Flow Control," in *6th AIAA Flow Control Conference, AIAA 2012-3137*, New Orleans, Louisiana, 25-28 June, 2012.

[9] T. Corke, C. Enloe and S. Wilkinson, "Dielectric Barrier Discharge Plasma Actuators for Flow Control,," *Annual Review of Fluid Mechanics*, vol. 42, pp. 505-529, 2010.

[10] M. Kotsonis, G. Correale, T. Michelis, D. Ragni and F. Scarano, ""Nanosecond-Pulsed Plasma Actuation in Quiescent Air and Laminar Boundary Layer," *Journal of Physics D: Applied Physics*, vol. 47, no. 10, p. 105201, 2014.

[11] J. Kriegseis, A. Duchmann, C. Tropea and S. Grundmann, "On the Classification of Dielectric Barrier Discharge Plasma Actuators: A Comprehensive Performance Evaluation Study," *Journal of Applied Physics,*, vol. 114, no. 053301, 2013.

[12] S. Leonov, D. Opaits, R. Miles and V. Soloviev, "Time-Resolved Measurements of Plasma-Induced Momentum in Air and Nitrogen Under Dielectric Barrier Discharge Actuation," *Physics of Plasmas*, vol. 17, no. 113505, 2010.

[13] E. Moreau, "Airflow Control by Non-thermal Plasma Actuators," *Journal of Physics D: Applied Physics*, vol. 40, pp. 605-636, 2007.

[14] S. Macheret, M. Shneider and R. and Miles, "Magnetohydrodynamic and Electrohydrodynamic Control of Hypersonic Flows of Weakly Ionized Plasmas," *AIAA Journal,*, vol. 42, no. 11, pp. 1378-1387, 2004.

[15] S. M., A. I., W. B., K. J., H. J. and P. P, "Development and Application of Localized Arc Filament Plasma Actuators for Jet Flow and Noise Control," in *42nd AIAA Aerospace Sciences Meeting and Exhibit, AIAA Paper 10.2514/6.2004-1*, Reno, Nevada, 2004.

[16] F. F., F. A.A., Y. D.A., G. M.A., T. K. and L. S.B., "Plasma Control of Shock Wave Configuration in Off-Design Mode of M = 2 inlet," *Experiments in Fluids,* 2015 56:54.

[17] R. Meyer, P. P, E. Ploenjes, J. W. Rich and I. V. Adamovich, "The Effect of a Nonequilibrium RF Discharge Plasma on a Conical Shock Wave in a M=2.5 Flow," *AIAA Journal,* vol. 41, no. 5, pp. 465-469, 2003.

[18] M. Minucci, P. Toro, A. Oliveira, A. Ramos, J. Chanes, A. Pereira, H. Nagamatsu, Leik and N. Myrabo, "Laser-Supported Directed Energy "Air Spike" in Hypersonic Flow," *Journal of Spacecraft and Rockets,* vol. 42, no. 1, pp. 51-57, 2005.

[19] S. Leonov, D. Yarantsev, A. Kuryachii and A. Yuriev, "Study of Friction and Separation Control by Surface Plasma," in *42nd AIAA Aerospace Sciences Meeting and Exhibit, AIAA-512*, Reno, Nevada, 2004.

[20] R. Adelgren, G. Elliot, J. Crawford, C. Carter, J. Donbar and D. Grosjean, "Axisymmetric Jet Shear-Layer Excitation Induced by Laser Energy and Electric Arc Discharges," *AIAA Journal,* vol. 43, no. 4, pp. 776-791, 2005.

[21] M. Samimy, I. Adamovich, B. Webb, J. Kastner, J. Hileman, S. Keshav and P. Palm, "Development and Characterization of Plasma Actuators for High Speed Jet Control," *Experiments in Fluids,* vol. 37, no. 4, pp. 577-588, 2004.

[22] S. Grundman and C. Tropea, "Experimental Damping of Boundary-Layer Oscillations Using DBD Plasma Actuators," *International Journal of Heat and Fluid Flow,* vol. 30, pp. 394-402, 2009.

[23] R. Hanson, P. Lavoie, A. Naguib and J. Morrison, "Transient Growth Instability Cancelation by a Plasma Actuator Array," *Experiments in Fluids,* vol. 49, no. 6, pp. 1339-1348, 2010.

[24] C. Rethmel, J. Little, K. Takashima, A. Sinha, I. Adamovich and M. and Samimy, "Flow Separation Control Using Nanosecond Pulse Driven DBD Plasma Actuators," *International Journal of Flow Control,* vol. 3, pp. 213-232, 2011.

[25] C. Porter, T. Mclaughlin, C. Enloe, G. Font, J. Roney and J. Baughn, "Boundary Layer Control Using a DBD Plasma Actuator," in *45th AIAA Aerospace Sciences Meeting and Exhibit, AIAA 2007-786* , Reno, Nevada., 2007.

[26] A. Kurz, S. Grundmann, C. Tropea, M. Forte, A. Seraudie, O. Vermeersch, D. Arnal, N. Goldin and R. King, "Boundary Layer Transition Control using DBD Plasma Actuators," *AerospaceLab Journal* , vol. 6, 2013.

[27] V. e. a. Kopiev, "Instability wave control in turbulent jet by plasma actuarors," *Journal of Physics D: Applied Physics,* vol. 47, p. 505201, 2014.

[28] S. Moralev, P. Boytsov and V. B. Kazansky, "Gas-dynamic Disturbances Created by Surface Dielectric Barrier Discharge in the Constricted Mode," *Experiments in Fluids,* vol. 55, no. 5, p. 1747, 2014.

[29] L. M. Mack, "Linear Stability Theory and the Problem of Supersonic Boundary- Layer Transition," *AIAA Journal,* vol. 13, no. 3, pp. 278-289, 1975.

[30] J. D. J. Anderson, "Hypersonic and High Temperature Gas Dynamics," in *Viscous Flow: Basic Aspects, Boundary Layer Results, and Aerodynamic Heating*, Reston, VA, American Institute of Aeronautics and Astronautics, Inc., 2000, p. chapter 6.

[31] N. L. Aleksandrov, S. V. Kidysheva, M. M. Nudnova and A. Y. Starikovskii, "Mechanism of Ultra-Fast Heating in a Non-Equilibrium Weakly Ionized Air Discharge Plasma in High Electric Fields," *Journal of Physics D: Applied Physics,* vol. 43, no. 255201, 2010.

[32] N. A. Popov, "Fast Gas Heating in a Nitrogen-Oxygen Discharge Plasma: I. Kinetic mechanism," *Journal of Physics D: Applied Physics,* vol. 44, no. 285201, 2011.

[33] I. Shkurenkov and I. Adamovich, "Energy Balance in Nanosecond Pulse Discharges in Nitrogen and Air," *Plasma Sources Science and Technology,* vol. 25, no. 015021, 2016.

[34] M. Nishihara, K. Takashima, J. Rich and I. Adamovich, "Mach 5 Bow Shock Control by a Nanosecond Pulse Surface Dielectric Barrier Discharge,"," *Physics of Fluids,* vol. 23, pp. 066101-1 – 066101-11, 2011.

[35] "NIST Chemical Kinetics Database," National Institute of Standards and Technology, [Online]. Available: http://kinetics.nist.gov/kinetics/.

[36] D. L. Rusterholtz, D. A. Lacoste, G. D. Stancu, D. Z. Pai and C. O. Laux, "Ultrafast Heating and Oxygen Dissociation in Atmospheric Pressure Air by Nanosecond Repetitively Pulsed Discharges," *Journal of Physics D: Applied Physics,* vol. 46, p. 464010, 2013.

[37] N. A. Popov, "Kinetic Processes Initiated by a Nanosecond High-Current Discharge in Hot Air," *Plasma Physics Reports*, vol. 37, pp. 805-817, 2011.

[38] N. A. Popov, "Investigation of the Mechanism for Rapid Heating of Nitrogen and Air in Gas Discharges," *Plasma Physics Reports*, vol. 27, no. 10, pp. 886-896, 2001.

[39] L. M. Mack, "Boundary Layer Linear Stability Theory," in *Special Course on Stability and Transition of Laminar Flow*, AGARD Report 709, 1984, pp. 1-81.

[40] A. Fedorov, A. Ryzhov and V. Soudakov, "Effect of Local Volume Energy Supply on High-Speed Boundary Layer Stability," in *43rd AIAA Fluid Dynamics Conference*, San Diego, California, 2013.

[41] S. Leonov, A. Houpt and F. Falempin, "Control of Hypersonic BL Transition by Electrical Discharge (feasibility study)," in *20th AIAA International Space Planes and Hypersonic Systems and Technologies Conference*, Glasgow, Scotland, 2015.

[42] Y. P. Raizer, Gas Discharge Physics, Berlin: Springer, 1991.

[43] R. K. Tyson, Principles of Adaptive Optics, New York: Academic., 1997.

[44] J. Sontag and S. Gordeyev, "Non-intrusive Velocity and Density Measurements in Subsonic Turbulent Boundary Layer," in *46th AIAA Plasmadynamics and Lasers Conference*, Dallas, Texas, 2015.

[45] A. Nightingale and S. Gordeyev, "Shack-Hartmann Wavefront Sensor Image Analysis: A Comparison of Centroiding Methods and Image Processing Techniques," *Journal of Optical Engineering*, vol. 52, no. 7, p. 071413, 2013.

[46] M. Wang, A. Mani and S. Gordeyev, "Physics and Computation of Aero-Optics," *Annual Review of Fluid Mechanics*, vol. 44, pp. 299-321, 2012.

[47] A. Houpt, S. Gordeyev, T. J. Juliano and S. B. Leonov, "Optical Measurement of Transient Plasma Impact on Corner Separation in M=4.5 Airflow," *Paper AIAA 2016-2160*, 2016.